European Journal of Pharmaceutics and Biopharmaceutics 133 (2018) 339–348

Contents lists available at ScienceDirect

European Journal of Pharmaceutics and Biopharmaceutics

journal homepage: www.elsevier.com/locate/ejpb

Research paper

siRNA-mediated protein knockdown in precision-cut lung slices

Mitchel J.R. Ruigrok[a], Jia-Ling Xian[a], Henderik W. Frijlink[a], Barbro N. Melgert[b], Wouter L.J. Hinrichs[a,*], Peter Olinga[a]

[a] University of Groningen, Groningen Research Institute of Pharmacy, Department of Pharmaceutical Technology and Biopharmacy, Antonius Deusinglaan 1, 9713 AV Groningen, the Netherlands

[b] University of Groningen, Groningen Research Institute of Pharmacy, Department of Pharmacokinetics, Toxicology, and Targeting, Antonius Deusinglaan 1, 9713 AV Groningen, the Netherlands

ARTICLE INFO

Keywords:
Explant culture
Gene silencing
Organotypic culture
Precision-cut tissue slices
Short interfering RNA
Transfection

ABSTRACT

Small interfering RNA (siRNA) can induce RNA interference, which leads to the knockdown of messenger RNA (mRNA) and protein. As a result, siRNA is often used *in vitro* and *in vivo* to unravel the function of genes and as a therapeutic agent to disrupt excessive expression of disease-related genes. However, there is a large gap between *in vitro* and *in vivo* models in terms of simplicity, flexibility, throughput, and translatability. This gap could be bridged by using precision-cut tissue slices, which represent viable explants prepared from animal or human tissue that can be cultured *ex vivo*. Previously, we demonstrated that self-deliverable siRNA (Accell siRNA) induced significant mRNA knockdown in lung slices. The goal of this study, however, was to investigate whether Accell siRNA also induced protein knockdown in murine lung slices. Slices were incubated for up to 96 h with no siRNA (untransfected), non-targeting siRNA (control), or gene-targeting siRNA (*Gapdh*, *Ppib*, *Serpinh1*, and *Bcl2l1*). Overall, untransfected and transfected slices remained viable during an incubation of 96 h. In addition, gene-targeting siRNAs induced not only significant and specific mRNA knockdown but also protein knockdown. Finally, protein knockdown of fibrogenesis-related targets (*Ppib*, *Serpinh1*, and *Bcl2l1*) was shown to influence fibrogenesis on mRNA level, thereby demonstrating this model its utility in functional genomics and translational research.

1. Introduction

Small interfering RNA (siRNA) is a class of double-stranded RNA molecules that can induce RNA interference (RNAi) – a process that leads to the transient knockdown of specific gene products, such as messenger RNA (mRNA) and protein [1]. Because siRNA can be used to knockdown virtually every gene, researchers can deduce the function of genes based on observed phenotypic changes [2]. siRNA can also be used therapeutically to disrupt excessive expression of disease-related genes, such as collagen expression in fibrosis or oncogene expression in cancer [3]. Although RNAi continues to be an indispensable tool in functional genomics and drug development, it remains crucial to select appropriate experimental models [4]. For example, there is a large translational gap between *in vitro* and *in vivo* models in terms of simplicity, flexibility, throughput, and translatability [5]. Novel experimental models, which combine advantages of *in vitro* and *in vivo* models, are therefore greatly desired.

This need could be addressed by using precision-cut tissue slices which are viable explants with a well-defined thickness and diameter, prepared from animal or human tissue (e.g. lungs, kidney, liver, and intestine), that can be cultured *ex vivo* [6]. An important advantage of this model is that the structural and functional heterogeneity of organs

Abbreviations: 18s, 18S ribosomal RNA; *Acta2*, Alpha smooth muscle actin (encodes protein α-SMA); ACTB, Beta-actin; ANOVA, Analysis of variance; ATP, Adenosine triphosphate; *Bcl2l1*, BCL2-like 1 (encodes protein BCL-XL); *Col1a1*, Collagen type 1 alpha 1 (encodes protein COL1A1); ECM, Extracellular matrix; ER, Endoplasmic reticulum; *Fn*, Fibronectin (encodes protein FN); *Gapdh*, Glyceraldehyde-3-phosphate dehydrogenase (encodes protein GAPDH); H&E, Hematoxylin and eosin; mRNA, Messenger RNA; *Ppib*, Peptidylprolyl isomerase B (encodes protein PPIB); qPCR, Real-time quantitative polymerase chain reaction; RNAi, RNA interference; SDS-PAGE, Sodium dodecyl sulfate-polyacrylamide gel electrophoresis; *Serpine1*, Serine (or cysteine) peptidase inhibitor clade E member 1 (encodes protein PAI-1); *Serpinh1*, Serine (or cysteine) peptidase inhibitor clade H member 1 (encodes protein HSP47); siRNA, Small interfering RNA; TGFβ1, Transforming growth factor β 1; *Tnfrsf11b*, Tumor necrosis factor receptor superfamily member 11b (encodes protein OPG); UW, University of Wisconsin; VCL, Vinculin; *Ywhaz*, Tyrosine 3-monooxygenase/tryptophan 5-monooxygenase activation protein zeta polypeptide (encodes protein 14-3-3ζ)

* Corresponding author.
E-mail address: w.l.j.hinrichs@rug.nl (W.L.J. Hinrichs).

https://doi.org/10.1016/j.ejpb.2018.11.005
Received 24 July 2018; Received in revised form 8 October 2018; Accepted 5 November 2018
Available online 07 November 2018
0939-6411/ © 2018 The Authors. Published by Elsevier B.V. This is an open access article under the CC BY license (http://creativecommons.org/licenses/BY/4.0/).

is conserved, partly due to the presence of cell-matrix and intercellular interactions. To that end, tissue slices appear to be a promising experimental model to assess the biological effects of siRNA in relevant biological environments. We previously demonstrated that self-deliverable siRNA (Accell siRNA) disrupted mRNA expression in lung and kidney slices prepared from murine tissue [5]. Although significant mRNA knockdown (55%) was achieved after an incubation of 48 h, protein knockdown was not observed (Supplementary Fig. 1). This discrepancy between mRNA and protein levels could have been caused by differences in their respective intracellular half-lives. Longer incubation times may be required for protein levels to reflect changes in mRNA levels.

Supplementary data associated with this article can be found, in the online version, at https://doi.org/10.1016/j.ejpb.2018.11.005.

Full potential of this transfection model can only be realized if knockdown of protein is also demonstrated. Therefore, the main goal of this study was to further characterize and optimize this transfection model to achieve protein knockdown in murine lung slices using Accell siRNA. First, we identified whether untransfected and transfected slices remained viable during an incubation of 96 h. The investigated viability parameters included the adenosine triphosphate (ATP), protein, and RNA content as well as morphology. Next, we analyzed whether various Accell siRNAs (targeting *Gapdh*, *Ppib*, *Serpinh1*, or *Bcl2l1*) induced mRNA and protein knockdown. mRNA knockdown was studied by real-time quantitative polymerase chain reaction (qPCR), whereas protein knockdown was investigated by western blotting. Finally, as *Ppib*, *Serpinh1*, and *Bcl2l1* are involved in fibrogenesis, we determined whether protein knockdown affected the fibrogenic phenotype of slices [7–9]. To that end, we assessed mRNA expression of the following markers: *Serpine1*, *Tnfrsf11b*, *Fn*, *Col1a1*, and *Acta2* [10–15].

2. Materials & methods

2.1. Animal tissue

Lung tissue was obtained from 8 to 12 weeks old C57BL/6J mice that were housed under controlled conditions with a 12 h light/dark cycle and free access to water and food (Central Animal Facility, University Medical Center Groningen, Groningen, The Netherlands). Prior to excision, the lungs were inflated *in situ* with liquefied and pre-warmed (37 °C) support medium containing 1.5% low-gelling-temperature agarose (Sigma-Aldrich, Zwijndrecht, The Netherlands) and 0.9% NaCl (Merck, Darmstadt, Germany) via a terminal procedure conducted under isoflurane/O_2 anesthesia (Nicolas Piramal, London, UK). Afterwards, the lungs were immediately transferred to ice-cold University of Wisconsin (UW) preservation solution (DuPont Critical Care, Waukegab, USA). All experiments were approved by the Animal Ethics Committee of the University of Groningen (permit no. 171290-01-001).

2.2. Precision-cut lung slices

As described previously, slices were made with a Krumdieck tissue slicer (Alabama Research and Development, Munford, USA), which was filled with ice-cold Krebs-Henseleit buffer supplemented with 25 mM D-glucose (Merck), 25 mM $NaHCO_3$ (Merck), and 10 mM HEPES (MP Biomedicals, Aurora, USA); saturated with carbogen (95% O_2 and 5% CO_2); and adjusted to a pH of 7.4 (Fig. 1) [5]. Lung slices had a wet weight of 4–5 mg, with an estimated thickness of 250–350 µm and a diameter of approximately 5 mm. Slices were incubated individually in 1 mL pre-warmed and oxygenated culture medium at 37 °C under 80% O_2 and 5% CO_2, while gently shaken (90 cycles per minute). Culture medium was composed of Accell siRNA Delivery Media (Dharmacon, Lafayette, USA) supplemented with 100 U/mL penicillin–streptomycin (Life Technologies, Bleiswijk, The Netherlands), 50 µg/mL gentamicin (Life Technologies), and 0.1 mM non-essential amino acids (Life Technologies). After slicing, slices were sampled directly or pre-incubated for 2 h in culture medium. Thereafter, slices were transferred to culture medium without Accell siRNA (untransfected) or with either 0.5 µM non-targeting (control) Accell siRNA or gene-targeting Accell siRNA (*Gapdh*, *Ppib*, *Serpinh1*, or *Bcl2l1*). All Accell siRNAs were purchased from Dharmacon. After 48 or 96 h of incubation, slices were collected for analysis.

2.3. ATP content

ATP was extracted from slices (3 per condition) using ice-cold sonication solution (70% ethanol and 2 mM EDTA) and a Minibead-beater for homogenization (1 cycle of 1.5 min). After centrifuging the homogenate (16,000*g* at 4 °C for 5 min), the supernatant was collected and subsequently analyzed using an ATP Bioluminescence Kit (Roche Diagnostics, Mannheim, Germany), as reported previously [6]. Obtained ATP values (pmol) were normalized to total amount of protein (µg), which was determined with the RC DC Protein Assay (Bio-Rad, Munich, Germany).

2.4. Morphology

After fixation in 4% formalin at 4 °C for 24 h, slices (3 per condition) were dehydrated in baths with increasing strengths of ethanol. Thereafter, slices were cleared in xylene baths and embedded horizontally in paraffin. Prior to staining with hematoxylin and eosin (H&E), sections (4 µm) were deparaffinized and rehydrated in baths with decreasing strengths of ethanol. Afterwards, sections were dehydrated in baths of increasing strengths of ethanol. Finally, slides were scanned with a C9600 NanoZoomer (Hamamatsu Photonics, Hamamatsu, Japan).

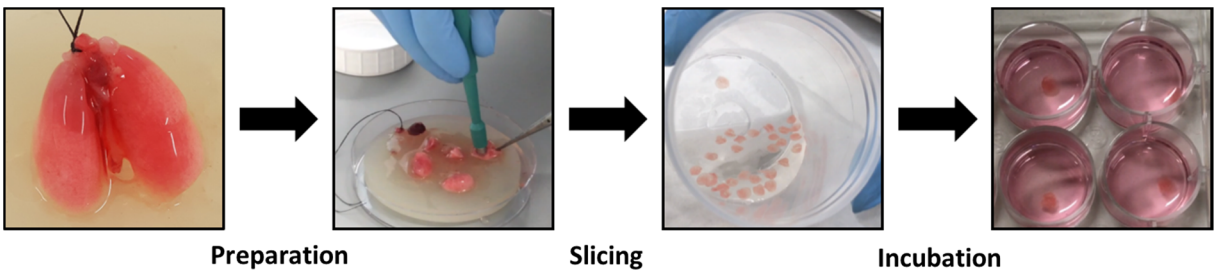

Fig. 1. Slicing workflow. Murine lungs were first inflated *in situ* with agarose and then excised. Cylindrical tissue cores were subsequently made using a biopsy puncher with a diameter of ~5 mm. Finally, slices were prepared with a Krumdieck tissue slicer, yielding slices with a thickness of 250–350 µm that can be cultured *ex vivo*.

Table 1
Primers.

Gene	Protein	Forward sequence (5′→3′)	Reverse sequence (5′→3′)
Acta2	α-SMA	ACTACTGCCGAGCGTGAGAT	CCAATGAAAGATGGCTGGAA
Bcl2l1	BCL-XL	ACATCCCAGCTTCACATAACCC	CCATCCCGAAAGAGTTCATTCAC
Col1a1	COL1A1	TGACTGGAAGAGCGGAGAGT	ATCCATCGGTCATGCTCTCT
Fn	FN	CGGAGAGAGTGCCCCTACTA	CGATATTGGTGAATCGCAGA
Gapdh	GAPDH	ACAGTCCATGCCATCACTGC	GATCCACGACGGACACATTG
Ppib	PPIB	GGCTCCGTCGTCTTCCTTTT	ACTCGTCCTACAGATTCATCTCC
Serpine1	PAI-1	GCCAGATTTATCATCAATGACTGGG	GGAGAGGTGCACATCTTTCTCAAAG
Serpinh1	HSP47	AGGTCACCAAGGATGTGGA	CAGCTTCTCCTTCTCGTCGT
Tnfrsf11b	OPG	ACAGTTTGCCTGGGACCAAA	CTGTGGTGAGGTTCGAGTGG
Ywhaz	14-3-3ζ	TTACTTGGCCGAGGTTGCT	TGCTGTGACTGGTCCACAAT

2.5. mRNA expression

Total RNA was isolated from slices (3 per condition) using a Maxwell 16 LEV SimplyRNA Tissue Kit (Promega, Leiden, The Netherlands) and the RNA yield was quantified with a BioTek Synergy HT (BioTek Instruments, Vermont, USA). Isolated RNA was subsequently reverse transcribed with the Reverse Transcription System (Promega), using a thermal cycler (22 °C for 10 min, 42 °C for 15 min, and 95 °C for 5 min). Next, mRNA expression was assessed by qPCR, using specific primers (Table 1) and FastStart Universal SYBR Green Master (Roche, Almere, The Netherlands). The analysis was performed with a ViiA7 real-time qPCR (Applied Biosystems, Bleiswijk, The Netherlands), using 1 cycle of 10 min at 95 °C and 40 cycles of 15 s at 95 °C, 30 s at 60 °C, and 30 s at 72 °C. mRNA expression was calculated as fold induction ($2^{-\Delta\Delta Ct}$ method), using *Ywhaz* as a reference gene.

2.6. Protein expression

GAPDH, PPIB, HSP47, and BCL-XL protein expression was determined by western blotting. In short, protein was extracted from slices (6–12 per condition) using ice-cold RIPA lysis buffer (Fischer Scientific, Landsmeer, The Netherlands) and a Minibead-beater for homogenization (five cycles of 45 s Minibead-beating and 10 min of cooling on ice). Samples were subsequently centrifuged (16,000*g* at 4 °C for 30 min) and denatured (75 °C for 15 min). Extracted protein (20 µg) was separated via sodium dodecyl sulfate–polyacrylamide gel electrophoresis (SDS-PAGE) using 10% gels and blotted onto polyvinylidene fluoride membranes using a Trans-Blot Turbo Transfer System (Bio-Rad). After blocking in 5% non-fat milk/TBST (Bio-Rad) for 1 h, membranes were incubated with the primary antibody (Table 2) overnight at 4 °C followed by incubation with the respective secondary antibody for 1 h. Thereafter, protein was visualized with Clarity Western ECL blotting substrate (Bio-Rad) using the ChemiDoc Touch Imaging System (Bio-Rad). Protein expression was normalized using housekeeping protein vinculin (VCL) as internal control.

2.7. Statistics

GraphPad Prism 6.0 was used to analyze data statistically using one-way analysis of variance (ANOVA) followed by either Tukey's multiple comparisons test to compare all means within a dataset or Dunnett's multiple comparisons test to compare all means with one control mean. Note, mRNA expression is shown as fold induction ($2^{-\Delta\Delta Ct}$), though the data was analyzed using the ΔCt values. Differences between groups were considered significant when $p < .05$.

3. Results

3.1. Viability of untransfected slices

First, the general viability and morphology of untransfected slices were characterized (Fig. 2). As such, we investigated the ATP/protein, protein, and RNA content as well as the morphology of untransfected slices at 0 h and after 48 and 96 h of incubation. The ATP/protein content was significantly higher after the first 48 h of culturing, after which it appeared to decrease again, albeit not significantly. Furthermore, both protein and RNA content significantly decreased over time. Generally, the morphology of slices remained good for up to 48 h. After 96 h, signs of moderate apoptosis manifested in the airways and parenchyma. In the airways, moderate karyolysis (nuclei dissolution), pyknosis (nuclei shrinkage), and karyorrhexis (nuclei fragmentation) were observed. Furthermore, in some cases, airway epithelial cells became squamous (flattened). Karyolysis, pyknosis, and karyorrhexis were also observed to a moderate extent in the parenchyma, along with some clusters of apoptotic bodies.

3.2. Viability of transfected slices

Next, we studied whether the use of Accell siRNA affected the viability of lung slices, after an incubation of 96 h, with a focus on ATP/protein, protein, and RNA content as well as morphology (Fig. 3). As

Table 2
Antibodies.

Protein	Primary antibody	Secondary antibody
BCL-XL (23 kDa)	Rabbit anti-BCL-XL (1:1000, Fischer Scientific)	Goat anti-rabbit HRP (1:2000, Dako, Santa Clara, USA)
GAPDH (36 kDa)	Mouse anti-GAPDH (1:5000, Sigma Aldrich)	Rabbit anti-mouse HRP (1:5000, Dako)
HSP47 (47 kDa)	Rabbit anti-HSP47 (1:2000, Abcam, Cambridge, USA)	Goat anti-rabbit HRP (1:2000, Dako)
PPIB (24 kDa)	Mouse anti-PPIB (1:1000, Fischer Scientific)	Rabbit anti-mouse HRP (1:5000, Dako)
VCL (116 kDa)	Mouse anti-VCL (1:500, Santa Cruz, California, USA)	Mouse binding protein HRP (1:1000, Santa Cruz)

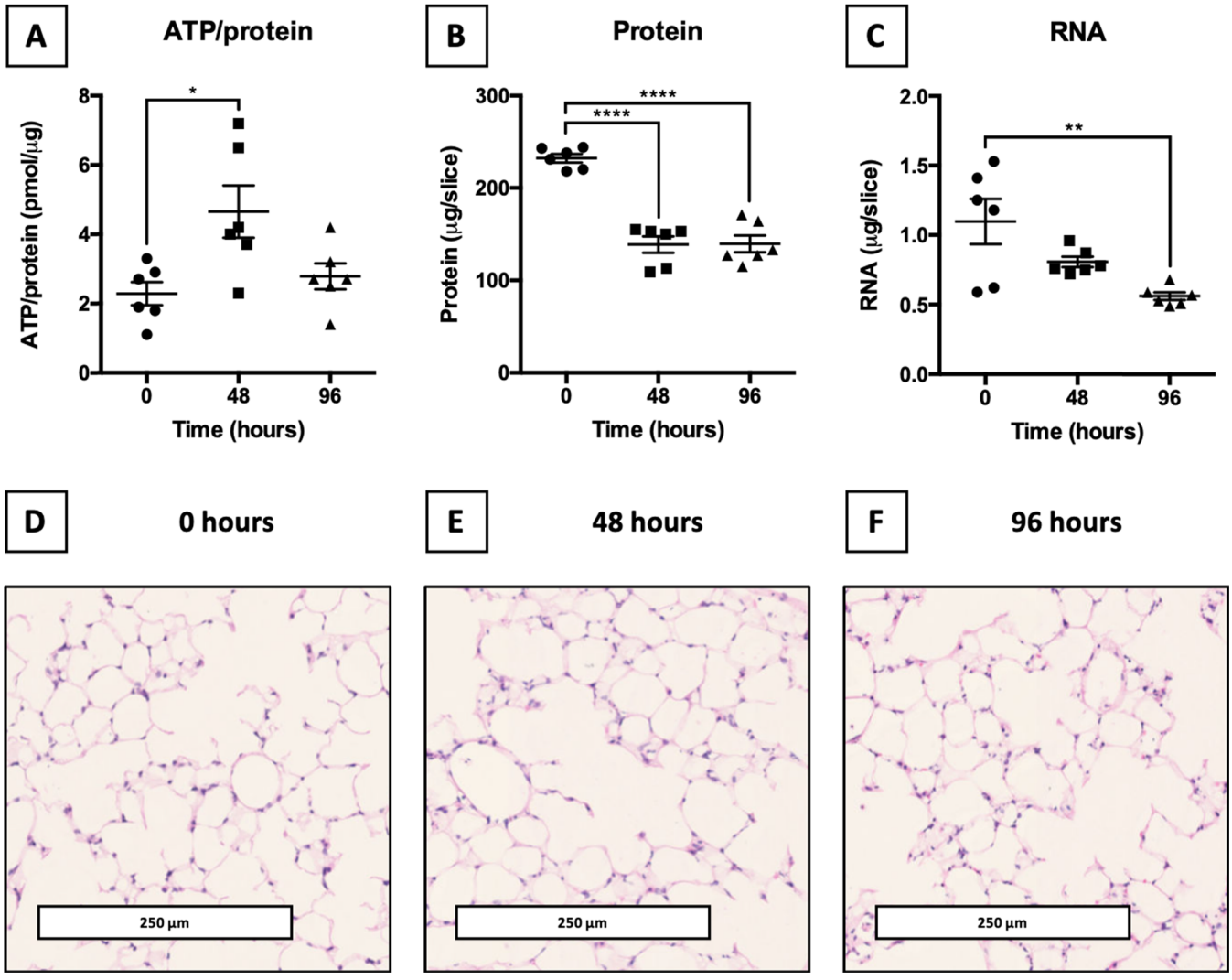

Fig. 2. Viability of untransfected slices. Untransfected slices were sampled after slicing (0 h) and after an incubation of 48 or 96 h (n = 3–6). Aside from ATP/protein (a), protein (b), and RNA (c) content, the general morphology (magnification 10×) was analyzed at 0 h (d), 48 h (e), and 96 h (f). Values represent individual experiments performed in triplicate and are accompanied with the arithmetic mean (horizontal line) ± standard error of the mean (error bars). Tukey's test was used to compare all means ($^{*}p < .05$, $^{**}p < .01$, and $^{****}p < .0001$).

illustrated, transfections with non-targeting, *Gapdh*-targeting, *Ppib*-targeting, *Serpinh1*-targeting, and *Bcl2l1*-targeting siRNA did not significantly change ATP/protein, protein, and RNA content in slices. Likewise, no substantial differences in the general morphology were observed between untransfected and transfected slices.

3.3. Baseline mRNA expression in untransfected slices

To avoid silencing genes that are (strongly) down- or upregulated during incubation, we determined whether the baseline mRNA expression of *Gapdh*, *Ppib*, *Serpinh1*, and *Bcl2l1* in untransfected lung slices remained stable during an incubation of up to 96 h (Fig. 4). As shown, the baseline expression of mRNAs targets did not significantly change over time.

3.4. mRNA knockdown in transfected slices

To determine whether RNA interference was induced, we analyzed *Gapdh*, *Ppib*, *Serpinh1*, and *Bcl2l1* mRNA expression in untransfected and transfected lung slices which were incubated for 96 h (Fig. 5). As demonstrated, *Gapdh*-targeting, *Ppib*-targeting, *Serpinh1*-targeting, and *Bcl2l1*-targeting siRNA induced significant and specific knockdown of respective target mRNAs (knockdown of 65, 95, 70, and 45%, respectively, compared to untransfected slices). Furthermore, no non-specific mRNA knockdown was observed with non-targeting siRNA.

3.5. Protein knockdown in transfected slices

GAPDH, PPIB, HSP47, and BCL-XL protein expression was studied to determine whether knockdown of the functional gene product was achieved after an incubation of 96 h (Fig. 6). As shown, *Gapdh*-targeting, *Ppib*-targeting, *Serpinh1*-targeting, and *Bcl2l1*-targeting siRNA resulted in significantly lower expression of corresponding protein targets by 70, 35, 75, and 50%, respectively, compared to untransfected slices. Furthermore, no non-specific protein knockdown was induced by non-targeting siRNA.

3.6. Fibrogenesis in untransfected slices

Prior to the actual application of this transfection model within the context of fibrogenesis, we determined the baseline mRNA expression of fibrogenesis-related genes (Fig. 7). As such, the mRNA expression of

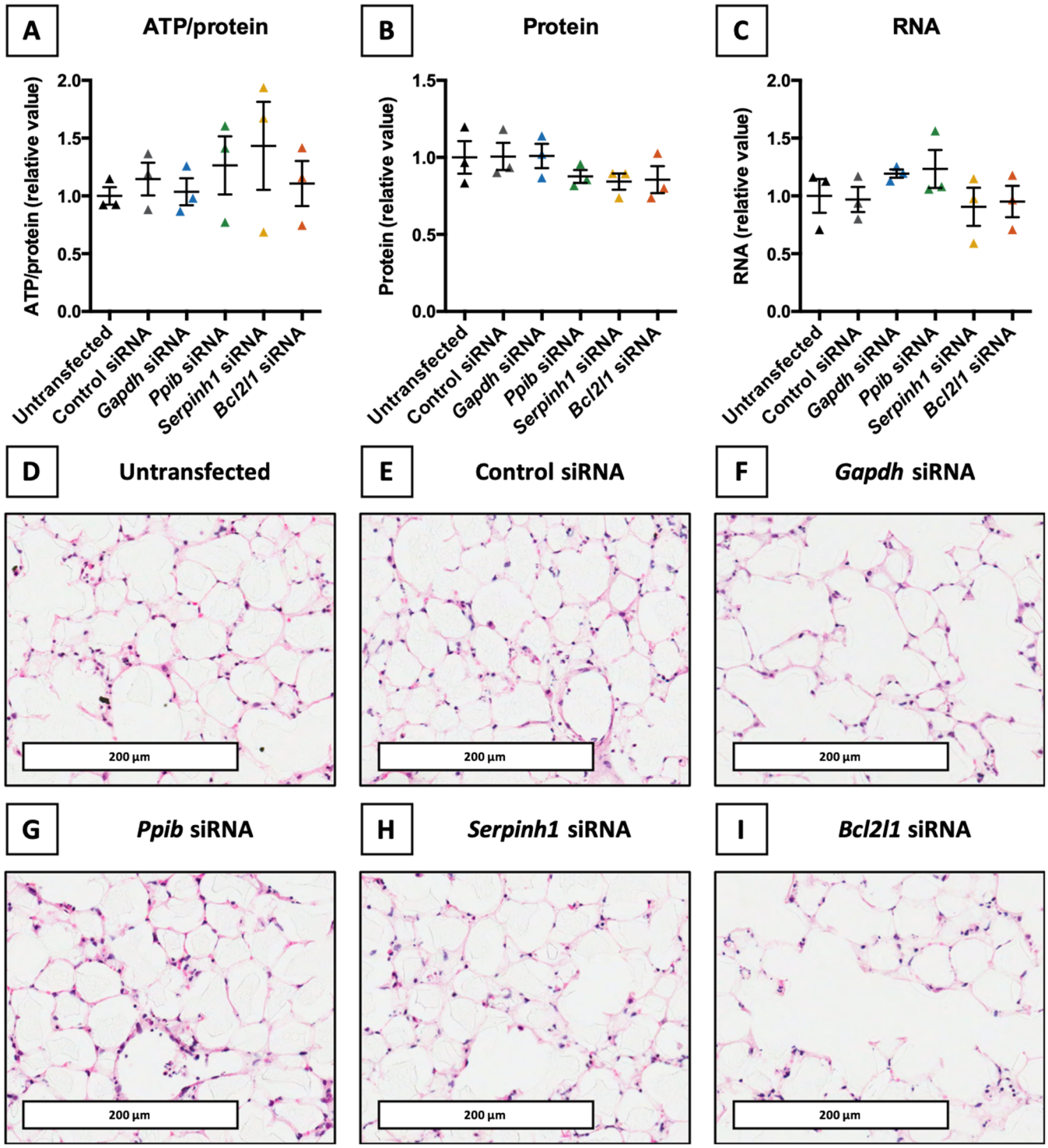

Fig. 3. Viability of transfected slices. Untransfected and transfected slices were sampled after an incubation of 96 h (n = 3). Thereafter, the ATP/protein (a), protein (b), and RNA (c) content of slices was assessed. In addition, the general morphology (magnification 10×) of untransfected slices (d) and slices transfected with non-targeting siRNA (e), *Gapdh*-targeting siRNA (f), *Ppib*-targeting siRNA (g), *Serpinh1*-targeting siRNA (h), and *Bcl2l1*-targeting siRNA (i) was analyzed. Values (relative to untransfected slices) represent individual experiments performed in triplicate and are accompanied with the arithmetic mean (horizontal line) ± standard error of the mean (error bars). Tukey's test was used to compare all means.

Serpine1, *Tnfrsf11b*, *Fn*, *Col1a1*, and *Acta2* was studied during an incubation of up to 96 h. Over time, mRNA expression of *Serpine1*, *Tnfrsf11b*, and *Fn* significantly increased, whereas expression of *Col1a1* and *Acta2* significantly decreased.

3.7. Fibrogenesis in transfected slices

Finally, we determined whether protein knockdown of PPIB, HSP47, and BCL-XL influenced the expression of fibrogenesis-related genes (Fig. 8). Therefore, *Serpine1*, *Tnfrsf11b*, *Fn*, *Col1a1*, and *Acta2*

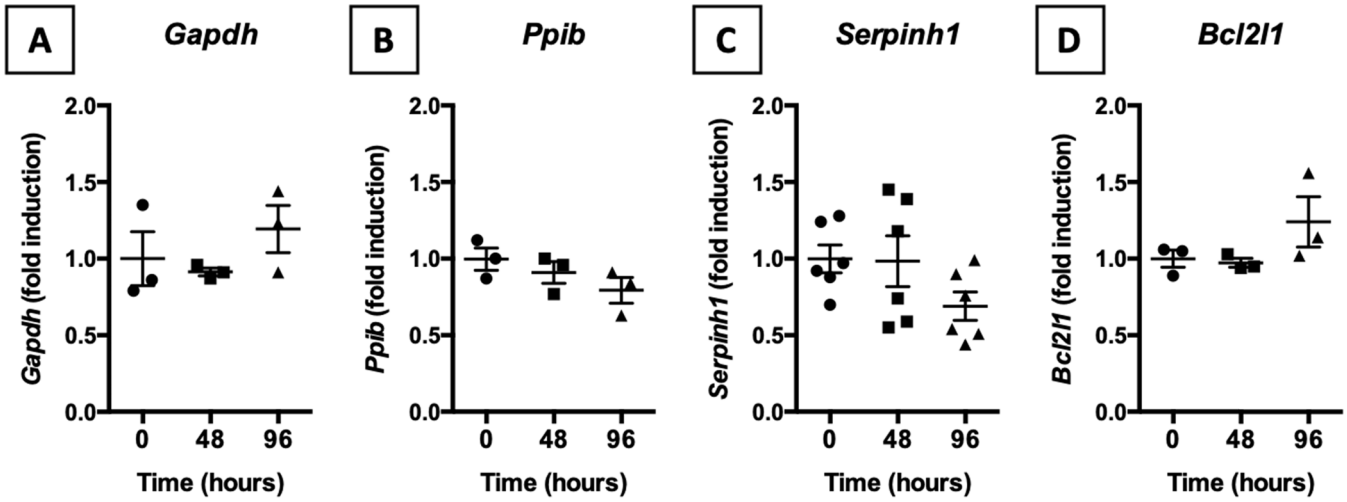

Fig. 4. Baseline mRNA expression in untransfected slices. Untransfected slices were sampled after slicing (0 h) and after an incubation of 48 or 96 h (n = 3–6). mRNA expression of *Gapdh* (a), *Ppib* (b), *Serpinh1* (c), and *Bcl2l1* (d) was analyzed by qPCR, using *Ywhaz* as a reference gene. Values represent individual experiments performed in triplicate and are accompanied with the arithmetic mean (horizontal line) ± standard error of the mean (error bars). Tukey's test was used to compare all means.

mRNA expression was examined in untransfected slices and slices treated with non-targeting, *Ppib*-targeting, *Serpinh1*-targeting, and *Bcl2l1*-targeting siRNA for 96 h. Compared to slices treated with non-targeting siRNA, slices treated with *Serpinh1*-targeting siRNA had significantly lower *Serpine1* and *Tnfrsf11b* mRNA expression, whereas treatment with *Ppib-targeting* and *Bcl2l1*-targeting siRNA only resulted in significantly lower *Tnfrsf11b* mRNA expression. *Fn*, *Col1a1*, and *Acta2* mRNA expression was not significantly different among the different groups.

4. Discussion

The main objective of this study was to investigate whether siRNA-mediated protein knockdown could be achieved in precision-cut lung slices using Accell siRNA. To this end, we first characterized viability parameters of lung slices and subsequently assessed effects of siRNA on mRNA and protein expression. In general, untransfected and transfected lung slices were shown to remain viable for up to 96 h, with moderate signs of apoptosis. More importantly, extending the incubation time to 96 h was shown to generate significant mRNA knockdown, which also resulted in knockdown of respective proteins. Furthermore, knockdown of PPIB, HSP47, and BCL-XL was shown to affect mRNA expression of fibrogenesis-related genes *Serpine1* and *Tnfrsf11b*, thereby demonstrating the utility of this transfection model to study the role of genes in a biologically relevant environment.

4.1. Viability

First of all, untransfected lung slices were characterized with respect to ATP/protein, protein, and RNA content as well as tissue morphology.

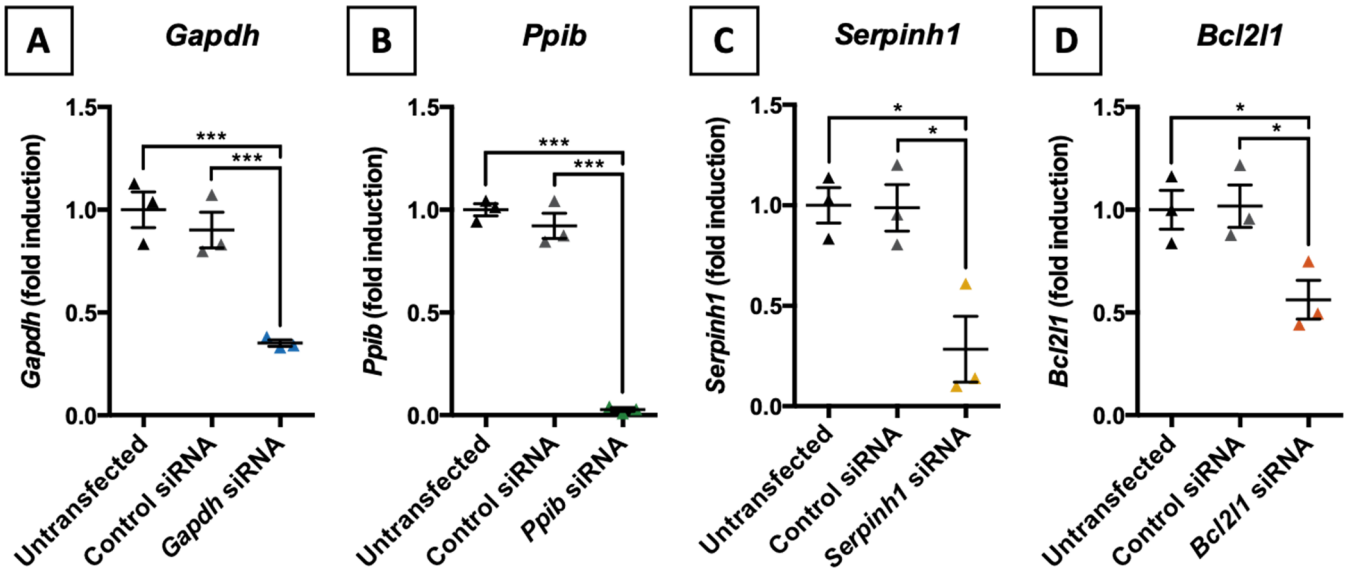

Fig. 5. mRNA knockdown in transfected slices. Untransfected and transfected slices were sampled after an incubation of 96 h (n = 3). mRNA knockdown of *Gapdh* (a), *Ppib* (b), *Serpinh1* (c), and *Bcl2l1* (d) was determined by qPCR, using *Ywhaz* as a reference gene. Values represent individual experiments performed in triplicate and are accompanied with the arithmetic mean (horizontal line) ± standard error of the mean (error bars). Tukey's test was used to compare all means ($^{*}p < .05$ and $^{***}p < .001$).

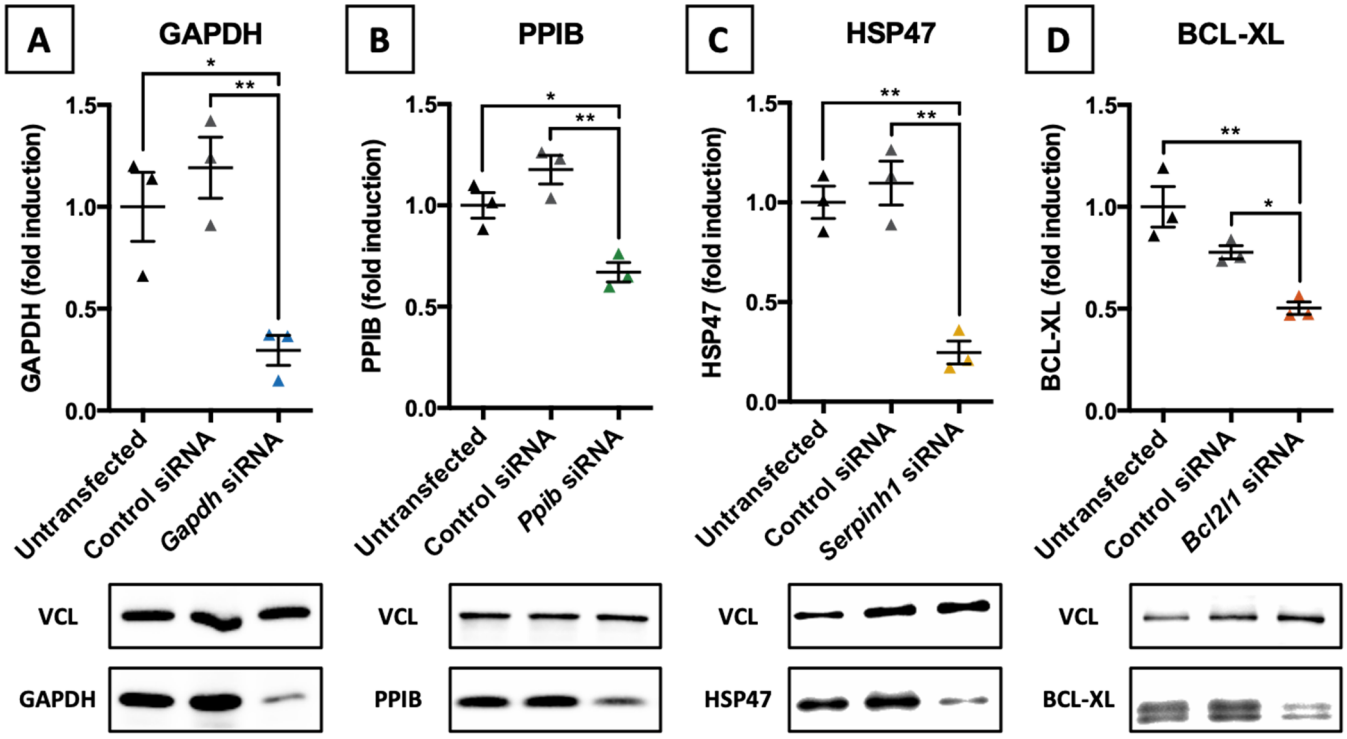

Fig. 6. Protein knockdown in transfected slices. Untransfected and transfected slices were sampled after an incubation of 96 h ($n = 3$). Protein knockdown of GAPDH (a), PPIB (b), HSP47 (c), and BCL-XL (d) was determined by western blotting, using VCL as a housekeeping protein. Values represent individual experiments performed in triplicate and are accompanied with the arithmetic mean (horizontal line) ± standard error of the mean (error bars). Tukey's test was used to compare all means ($^{*}p < .05$ and $^{**}p < .01$).

Although ATP/protein levels in untransfected slices remained relatively stable over time, the protein and RNA content decreased which suggests a fraction of cells disappeared (e.g., due to apoptosis) while the remaining cells remained viable. Morphological analyses of untransfected slices revealed similar observations because moderate pyknosis (irreversible condensation of chromatin) and karyorrhexis (fragmentation of nuclei) were observed after 96 h of incubation. In line with our previous study, signs of apoptosis were not observed after an incubation of 48 h [5]. Other publications describe permissible incubation times for lung slices ranging from 24 h up to 15 days, though different viability parameters were studied [16–21]. This makes comparisons particularly difficult because not all viability parameters are equally informative.

More importantly, no significant differences were observed in ATP/protein, protein content, and RNA content between untransfected and transfected slices after 96 h of incubation. The tissue morphology was not affected by siRNA transfections either. Previously, we showed Accell siRNA could be used to transfect murine lung slices (and kidney slices) without affecting the viability after 48 h of incubation [5]. This study complements those findings by demonstrating that lung slices could be incubated with Accell siRNA for an extended period of time

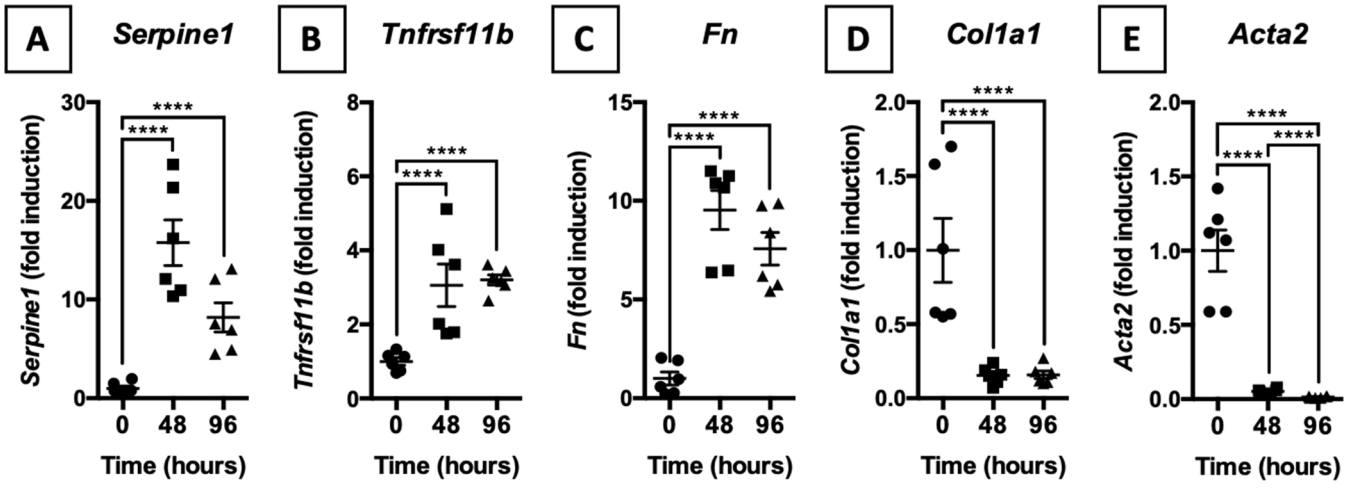

Fig. 7. Fibrogenesis in untransfected slices. Untransfected slices were sampled after slicing (0 h) and after an incubation of 48 or 96 h ($n = 6$). mRNA expression of *Serpine1* (a), *Tnfrsf11b* (b), *Fn* (c), *Col1a1* (d), and *Acta2* (e) were analyzed by qPCR, using *Ywhaz* as a reference gene. Values represent individual experiments performed in triplicate and are accompanied with the arithmetic mean (horizontal line) ± standard error of the mean (error bars). Tukey's test was used to compare all means ($^{****}p < .0001$).

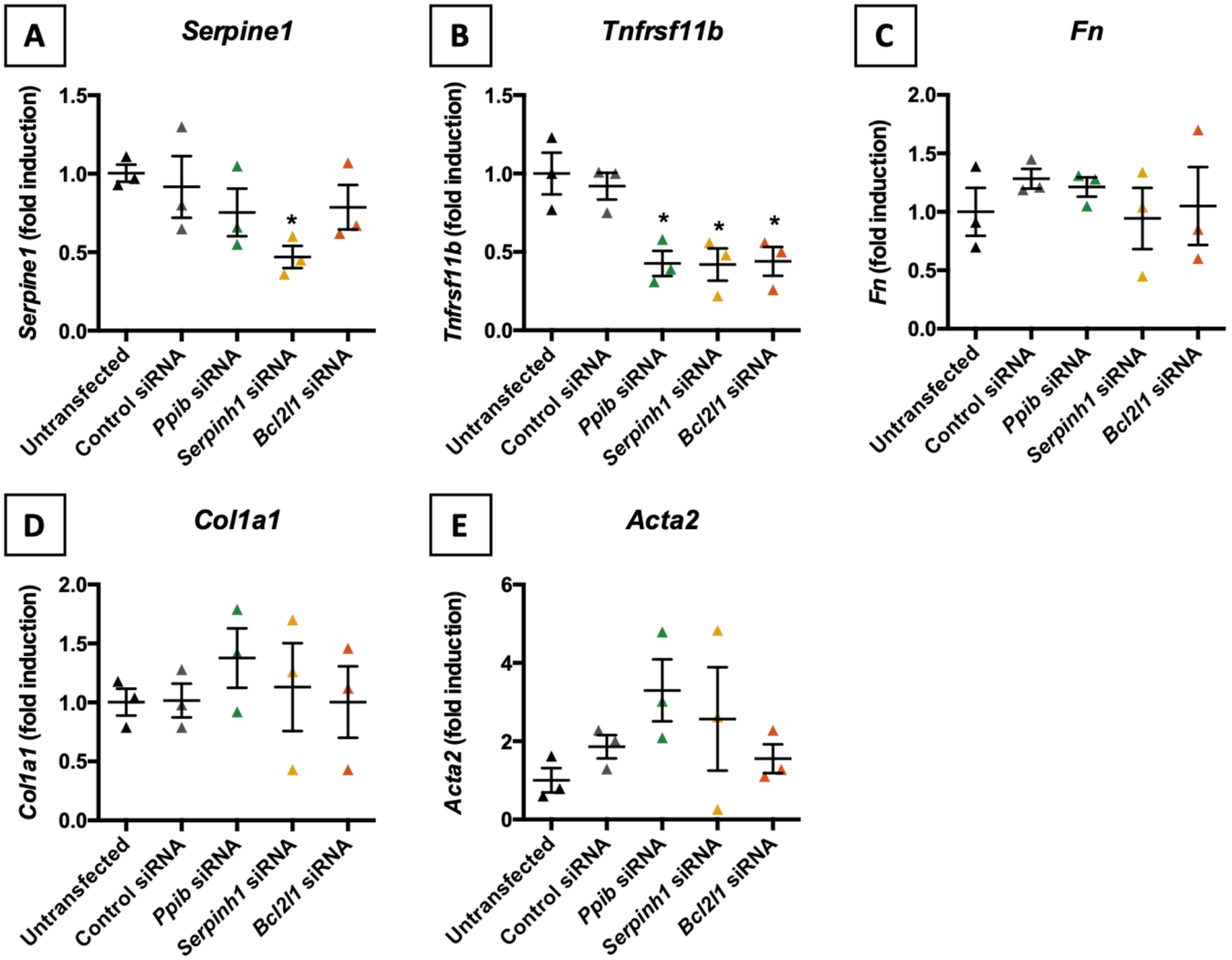

Fig. 8. Fibrogenesis in transfected slices. Untransfected and transfected lung slices were sampled after an incubation of 96 h (n = 3). Next, mRNA expression of *Serpine1* (a), *Tnfrsf11b* (b), *Fn* (c), *Col1a1* (d), and *Acta2* (e) was analyzed by qPCR, using *Ywhaz* as a reference gene. Values represent individual experiments performed in triplicate and are accompanied with the arithmetic mean (horizontal line) ± standard error of the mean (error bars). Dunnett's test was used to compare means vs. non-targeting siRNA ($^{*}p < .05$).

(96 h). This finding is important as commonly used membrane-disruption-mediated (e.g., optoporation, electroporation, and micro-injections) and carrier-mediated (e.g., viral vectors, lipid-based nanoparticles, and polymer-based nanoparticles) transfection technologies can have profound cytotoxic effects [22]. Obviously, though the viability of slices was not affected by the Accell siRNAs, care should be taken not to extrapolate these findings to all potential siRNA targets. For example, highly efficient knockdown of crucial proteins can potentially have detrimental effects on the viability of slices.

4.2. Knockdown

After confirming stable mRNA expression of *Gapdh*, *Ppib*, *Serpinh1*, and *Bcl2l1* during an incubation of up to 96 h, we observed significant and specific mRNA knockdown of respective targets using Accell siRNA. Results presented here build on our previous work by demonstrating the utility of Accell siRNA to induce transient knockdown of not only *Gapdh* but also *Ppib*, *Serpinh1*, and *Bcl2l1* [5]. Regarding mRNA knockdown, we observed different efficiencies between the tested siRNAs. Sources of variation could involve the abundance of targeted

Table 3
Fibrogenesis-related genes.

Gene	Expression	Function	Reference
Acta2	(Myo)fibroblasts	Encodes a smooth-muscle protein which promotes wound-repair by contracting edges of wounds	Longo et al. (2015) [15]
Col1a1	(Myo)fibroblasts	Encodes an important extracellular matrix (ECM) constituent to support closure of wounds	Wynn et al. (2012) [14]
Fn	(Myo)fibroblasts	Encodes a glycoprotein of the ECM which operates as a ligand for cell surface receptors	Bonnans et al. (2014) [13]
Serpine1	Endothelial cells (Myo)fibroblasts	Encodes a serine protease inhibitor that shields ECM proteins from proteolytic degradation	Ghosh et al. (2012) [10]
Tnfrsf11b	(Myo)fibroblasts Smooth muscle cells	Encodes a biomarker for transforming growth factor β 1 (TGFβ1) pathway activation	Simionescu et al. (2007) [11] Toffoli et al. (2011) [12]

mRNA, the efficiency of siRNA sequences, and the applicability of feedback mechanisms. For example, although siRNA-mediated RNAi is a catalytic process, knockdown does depend on the number of mRNA copies – fewer copies are more easily degraded than many copies [23]. Furthermore, the siRNA sequence determines the position where mRNA cleavage will occur. Depending on the local secondary structure of mRNA, cleavage can be hampered or promoted [24,25]. Lastly, feedback mechanisms, such as micro RNA (miRNA) expression and transcriptional activation, could be triggered upon siRNA-mediated mRNA knockdown to compensate for changes in mRNA levels [26,27]. These factors, or a combination thereof, could have contributed to differences in the extent of mRNA knockdown.

Moreover, we observed significant and specific protein knockdown in lung slices after an incubation of 96 h. As a result, this transfection model can be applied to study the effects of siRNA in a relevant biological environment. Interestingly, except for slices treated with *Ppib*-targeting siRNA, protein knockdown after 96 h was approximately similar to respective mRNA knockdown, thereby suggesting equilibration. Equilibration between mRNA and protein depends on the intracellular half-life, which is determined by protein degradation kinetics [28]. Perhaps PPIB has a longer intracellular half-life than GAPDH, HSP47, and BCL-XL. Usually, secreted proteins have different *in vitro* degradation kinetics than cytoplasmic proteins. Secreted proteins are generally degraded via lysosomal degradation, whereas cytoplasmic proteins are degraded by the ubiquitin-proteasome system [29]. Unlike GAPDH, HSP47, and BCL-XL, the protein PPIB can be secreted by cells via the constitutive secretory pathway either spontaneously or as a response to oxidative stress [8,9,30,31]. As such, it is possible that relevant amounts of PPIB resided in intracellular vesicles ready for secretion, thus avoiding degradation by the ubiquitin-proteasome system. Further exploration of specific PPIB degradation kinetics, however, was beyond the scope of this study.

4.3. Fibrogenesis

As mentioned earlier, we determined whether protein knockdown of PPIB, HSP47, and BCL-XL affected the fibrogenic phenotype of slices. First, we assessed the baseline expression of fibrogenesis-related genes, such as *Acta2*, *Col1a1*, *Fn*, *Serpine1*, and *Tnfrsf11b* (Table 3). As demonstrated, mRNA expression of *Serpine1*, *Tnfrsf11b*, and *Fn* significantly increased, whereas mRNA expression of *Col1a1* and *Acta2* significantly decreased. This response could have been induced by the release of pro-fibrogenic factors (e.g., growth factors, proteases, and metalloproteinases) from the extracellular matrix (ECM) into culture medium as well as by the release of cytokines by cells. As the slicing process partially disrupts the ECM, such factors could have diffused into the medium, potentially leading to activation of, for example, the transforming growth factor β 1 (TGFβ1) signaling pathway – one of the key drivers of fibrogenesis [32,33]. Clearly, these changes in mRNA expression may not fully reflect changes in the expression of functional gene products (i.e., proteins) but it does provide an indication of an early fibrogenic response. Lung slices are therefore particularly useful in fibrosis-related research because they display early signs of fibrogenesis as well as acute inflammation, which we observed in our previous study [5].

Finally, we determined whether knockdown of PPIB, HSP47, and BCL-XL affected the mRNA expression of fibrogenesis-related genes. As shown, only *Serpine1* and *Tnfrsf11b* mRNA expression was significantly affected. Though further elucidation of causative mechanisms was beyond the scope of this particular study, we could speculate on relevant mechanisms. For instance, HSP47 is necessary for the appropriate intracellular folding and trafficking of collagen type 1 in myofibroblasts, which are key effector cells in fibrogenesis. Accordingly, the knockdown of HSP47 leads to the accumulation of misfolded procollagens in the endoplasmic reticulum (ER) [34]. Recent research has shown that HSP47 knockdown induced ER-stress mediated apoptosis in myofibroblasts, thereby leading to a lower expression of TGFβ1 [8,35]. A lowered expression of TGFβ1 could have led to a lowered mRNA expression of *Serpine1* and *Tnfrsf11b* because these genes are involved in fibrogenesis [10–12]. Nonetheless, although no major inferences can be made regarding the downstream effects of PPIB, HSP47, and BCL-XL knockdown in fibrogenesis, the data does illustrate that siRNA-mediated protein knockdown can induce phenotypic changes in lung slices, thereby demonstrating the potential of this *ex vivo* transfection model. To go a step further, the same transfection technique could be applied to slices prepared from human lung tissue. The preparation of human lung slices is similar to the slicing procedure presented here, as described by others [36,37]. Briefly, after careful inflation of human lung tissue with agarose via the airways, cylindrical tissue cores can be prepared with a biopsy puncher, after which slices can be prepared using a Krumdieck tissue slicer. As a result, the use of human lung tissue makes this transfection technique even more relevant in translational research.

5. Conclusion

The principle aim of this present work was to further characterize and optimize an siRNA transfection model for lung slices to achieve protein knockdown using Accell siRNA. Overall, lung slices remained viable after an incubation of 96 h, though signs of apoptosis were observed. In addition, the viability of slices was not significantly affected by transfections with Accell siRNA. More importantly, gene-targeting siRNAs induced not only significant and specific knockdown of mRNA levels but also knockdown of respective proteins. In the context of fibrogenesis, this model was also applied to study whether protein knockdown resulted in phenotypic changes. As shown, PPIB, HSP47, and BCL-XL knockdown affected mRNA expression of fibrogenesis-related genes (*Serpine1* and *Tnfrsf11b*). Collectively, the results illustrate that this *ex vivo* transfection model can be used to study the effects of siRNA in a biologically relevant environment. Moreover, the same transfection technique could be applied to lung slices prepared from human tissue, thereby further expanding the model its utility in translational research.

References

[1] G.J. Hannon, RNA interference, Nature 418 (2002) 244–251, https://doi.org/10.1038/418244a.
[2] C. Fellmann, S.W. Lowe, Stable RNA interference rules for silencing, Nat. Cell Biol. 16 (2013) 10–18, https://doi.org/10.1038/ncb2895.
[3] C. Jiménez Calvente, A. Sehgal, Y. Popov, Y.O. Kim, V. Zevallos, U. Sahin, et al., Specific hepatic delivery of procollagen α1(I) small interfering RNA in lipid-like nanoparticles resolves liver fibrosis, Hepatology 62 (2015) 1285–1297, https://doi.org/10.1002/hep.27936.
[4] M.J.R. Ruigrok, H.W. Frijlink, W.L.J. Hinrichs, Pulmonary administration of small interfering RNA: the route to go? J. Control. Release 235 (2016) 14–23, https://doi.org/10.1016/j.jconrel.2016.05.054.
[5] M.J.R. Ruigrok, N. Maggan, D. Willaert, H.W. Frijlink, B.N. Melgert, P. Olinga, et al., siRNA-mediated RNA interference in precision-cut tissue slices prepared from mouse lung and kidney, AAPS J. 19 (2017) 1855–1863, https://doi.org/10.1208/s12248-017-0136-y.
[6] I.A.M. de Graaf, P. Olinga, M.H. de Jager, M.T. Merema, R. de Kanter, E.G. van de Kerkhof, et al., Preparation and incubation of precision-cut liver and intestinal slices for application in drug metabolism and toxicity studies, Nat. Protoc. 5 (2010) 1540–1551, https://doi.org/10.1038/nprot.2010.111.
[7] W.A. Cabral, I. Perdivara, M.A. Weis, M. Terajima, A.R. Blissett, W. Chang, et al., Abnormal type I collagen post-translational modification and crosslinking in a cyclophilin B KO mouse model of recessive osteogenesis imperfecta, PLoS Genet. 10 (2014), https://doi.org/10.1371/journal.pgen.1004465.
[8] M. Otsuka, M. Shiratori, H. Chiba, K. Kuronuma, Y. Sato, Y. Niitsu, et al., Treatment of pulmonary fibrosis with siRNA against a collagen-specific chaperone HSP47 in vitamin A-coupled liposomes, Exp. Lung Res. 43 (2017) 271–282, https://doi.org/10.1080/01902148.2017.1354946.
[9] D. Lagares, A. Santos, P.E. Grasberger, F. Liu, C.K. Probst, R.A. Rahimi, et al., Targeted apoptosis of myofibroblasts with the BH3 mimetic ABT-263 reverses established fibrosis, Sci. Transl. Med. 9 (2017) eaal3765, https://doi.org/10.1126/scitranslmed.aal3765.
[10] A.K. Ghosh, D.E. Vaughan, PAI-1 in tissue fibrosis, J. Cell. Physiol. 227 (2012) 493–507, https://doi.org/10.1002/jcp.22783.

[11] A. Simionescu, D.T. Simionescu, N.R. Vyavahare, Osteogenic responses in fibroblasts activated by elastin degradation products and transforming growth factor-β1: role of myofibroblasts in vascular calcification, Am. J. Pathol. 171 (2007) 116–123, https://doi.org/10.2353/ajpath.2007.060930.
[12] B. Toffoli, R.J. Pickering, D. Tsorotes, B. Wang, S. Bernardi, P. Kantharidis, et al., Osteoprotegerin promotes vascular fibrosis via a TGF-β1 autocrine loop, Atherosclerosis. 218 (2011) 61–68, https://doi.org/10.1016/j.atherosclerosis.2011.05.019.
[13] C. Bonnans, J. Chou, Z. Werb, Remodelling the extracellular matrix in development and disease, Nat. Rev. Mol. Cell Biol. 15 (2014) 786–801, https://doi.org/10.1038/nrm3904.
[14] T.A. Wynn, T.R. Ramalingam, Mechanisms of fibrosis: therapeutic translation for fibrotic disease, Nat. Med. 18 (2012) 1028–1040, https://doi.org/10.1038/nm.2807.
[15] D.L. Longo, D.C. Rockey, P.D. Bell, J.a. Hill, Fibrosis – a common pathway to organ injury and failure, N. Engl. J. Med. 372 (2015) 1138–1149, https://doi.org/10.1056/NEJMra1300575.
[16] M. Nassimi, C. Schleh, H.D.D. Lauenstein, R. Hussein, H.G.G. Hoymann, W. Koch, et al., A toxicological evaluation of inhaled solid lipid nanoparticles used as a potential drug delivery system for the lung, Eur. J. Pharm. Biopharm. 75 (2010) 107–116, https://doi.org/10.1016/j.ejpb.2010.02.014.
[17] N.U.B. Hansen, M.A. Karsdal, S. Brockbank, S. Cruwys, S. Rønnow, D.J. Leeming, et al., Tissue turnover of collagen type I, III and elastin is elevated in the PCLS model of IPF and can be restored back to vehicle levels using a phosphodiesterase inhibitor, Respir. Res. 17 (2016) 76, https://doi.org/10.1186/s12931-016-0394-8.
[18] V.A. Lambermont, M. Schlepütz, C. Dassow, P. König, L.J. Zimmermann, S. Uhlig, et al., Comparison of airway responses in sheep of different age in precision-cut lung slices (PCLS), PLoS ONE 9 (2014) e97610, https://doi.org/10.1371/journal.pone.0097610.
[19] I. Dobrescu, B. Levast, K. Lai, M. Delgado-Ortega, S. Walker, S. Banman, et al., In vitro and ex vivo analyses of co-infections with swine influenza and porcine reproductive and respiratory syndrome viruses, Vet. Microbiol. 169 (2014) 18–32, https://doi.org/10.1016/j.vetmic.2013.11.037.
[20] H.P. Behrsing, M.J. Furniss, M. Davis, J.E. Tomaszewski, R.E. Parchment, In vitro exposure of precision-cut lung slices to 2-(4-amino-3-methylphenyl)-5-fluorobenzothiazole lysylamide dihydrochloride (NSC 710305, Phortress) increases inflammatory cytokine content and tissue damage, Toxicol. Sci. 131 (2013) 470–479, https://doi.org/10.1093/toxsci/kfs319.
[21] V. Neuhaus, D. Schaudien, T. Golovina, U.-A. Temann, C. Thompson, T. Lippmann, et al., Assessment of long-term cultivated human precision-cut lung slices as an ex vivo system for evaluation of chronic cytotoxicity and functionality, J. Occup. Med. Toxicol. 12 (2017) 13, https://doi.org/10.1186/s12995-017-0158-5.
[22] M.P. Stewart, A. Sharei, X. Ding, G. Sahay, R. Langer, K.F. Jensen, In vitro and ex vivo strategies for intracellular delivery, Nature 538 (2016) 183–192, https://doi.org/10.1038/nature19764.
[23] A. Arvey, E. Larsson, C. Sander, C.S. Leslie, D.S. Marks, Target mRNA abundance dilutes microRNA and siRNA activity, Mol. Syst. Biol. 6 (2010) 1–7, https://doi.org/10.1038/msb.2010.24.
[24] K.Q. Luo, D.C. Chang, The gene-silencing efficiency of siRNA is strongly dependent on the local structure of mRNA at the targeted region, Biochem. Biophys. Res. Commun. 318 (2004) 303–310, https://doi.org/10.1016/j.bbrc.2004.04.027.
[25] Y. Pei, T. Tuschl, On the art of identifying effective and specific siRNAs, Nat. Methods 3 (2006) 670–676, https://doi.org/10.1038/nmeth911.
[26] R.C. Wilson, J.A. Doudna, Molecular mechanisms of RNA interference, Annu. Rev. Biophys. 42 (2013) 217–239, https://doi.org/10.1146/annurev-biophys-083012-130404.
[27] L.-C. Li, S.T. Okino, H. Zhao, D. Pookot, R.F. Place, S. Urakami, et al., Small dsRNAs induce transcriptional activation in human cells, Proc. Natl. Acad. Sci. 103 (2006) 17337–17342, https://doi.org/10.1073/pnas.0607015103.
[28] I.V. Hinkson, J.E. Elias, The dynamic state of protein turnover: it's about time, Trends Cell Biol. 21 (2011) 293–303, https://doi.org/10.1016/j.tcb.2011.02.002.
[29] S. Rothman, How is the balance between protein synthesis and degradation achieved? Theor. Biol. Med. Model. 7 (2010) 25, https://doi.org/10.1186/1742-4682-7-25.
[30] J.-Y. Zhang, F. Zhang, C.-Q. Hong, A.E. Giuliano, X.-J. Cui, G.-J. Zhou, et al., Critical protein GAPDH and its regulatory mechanisms in cancer cells, Cancer Biol. Med. 12 (2015) 10–22, https://doi.org/10.7497/j.issn.2095-3941.2014.0019.
[31] H. Hoffmann, C. Schiene-Fischer, Functional aspects of extracellular cyclophilins, Biol. Chem. 395 (2014) 721–735, https://doi.org/10.1515/hsz-2014-0125.
[32] R.J. Akhurst, A. Hata, Targeting the TGFβ signalling pathway in disease, Nat. Rev. Drug Discov. 11 (2012) 790–811, https://doi.org/10.1038/nrd3810.
[33] C.E. Boorsma, B.G.J. Dekkers, E.M. van Dijk, K. Kumawat, J. Richardson, J.K. Burgess, et al., Beyond TGFβ – novel ways to target airway and parenchymal fibrosis, Pulm. Pharmacol. Ther. 29 (2014) 166–180, https://doi.org/10.1016/j.pupt.2014.08.009.
[34] T. Taguchi, M.S. Razzaque, The collagen-specific molecular chaperone HSP47: is there a role in fibrosis? Trends Mol. Med. 13 (2007) 45–53, https://doi.org/10.1016/j.molmed.2006.12.001.
[35] K. Kawasaki, R. Ushioda, S. Ito, K. Ikeda, Y. Masago, K. Nagata, Deletion of the collagen-specific molecular chaperone Hsp47 causes endoplasmic reticulum stress-mediated apoptosis of hepatic stellate cells, J. Biol. Chem. 290 (2015) 3639–3646, https://doi.org/10.1074/jbc.M114.592139.
[36] A.D. Rieg, S. Suleiman, A. Perez-Bouza, T. Braunschweig, J.W. Spillner, T. Schroder, et al., Milrinone relaxes pulmonary veins in guinea pigs and humans, PLoS ONE 9 (2014) e87685, https://doi.org/10.1371/journal.pone.0087685.
[37] L. Wujak, C. Hesse, K. Sewald, D. Jonigk, P. Braubach, G. Warnecke, et al., FXII promotes proteolytic processing of the LRP1 ectodomain, Biochim. Biophys. Acta - Gen. Subj. 2017 (1861) 2088–2098, https://doi.org/10.1016/j.bbagen.2017.05.023.